SHREC'19: Shape Correspondence with Isometric and Non-Isometric Deformations

R. M. Dyke[1]*, C. Stride[1]*, Y.-K. Lai[1]*, P. L. Rosin[1]*, M. Aubry[2], A. Boyarski[3], A. M. Bronstein[3], M. M. Bronstein[4], D. Cremers[5], M. Fisher[6], T. Groueix[2], D. Guo[7], V. G. Kim[6], R. Kimmel[3], Z. Lähner[5], K. Li[7], O. Litany[8], T. Remez[9], E. Rodolà[10], B. C. Russell[6], Y. Sahillioğlu[11], R. Slossberg[3], G. K. L. Tam[12], M. Vestner[5], Z. Wu[7], J. Yang[7]

[1]School of Computer Science and Informatics, Cardiff University, UK
[2]LIGM, École des Ponts ParisTech, Universite Paris Est, France
[3]Department of Computer Science, Israel Institute of Technology, Israel
[4]Department of Computing, Imperial College London, UK
[5]Department of Computer Science, TU Munich, Germany
[6]Adobe Research
[7]Tianjin University, China
[8]Facebook AI Research
[9]School of Electrical Engineering, Tel-Aviv University, Israel
[10]Computer Science, Sapienza University of Rome, Italy
[11]Middle East Technical University, Turkey
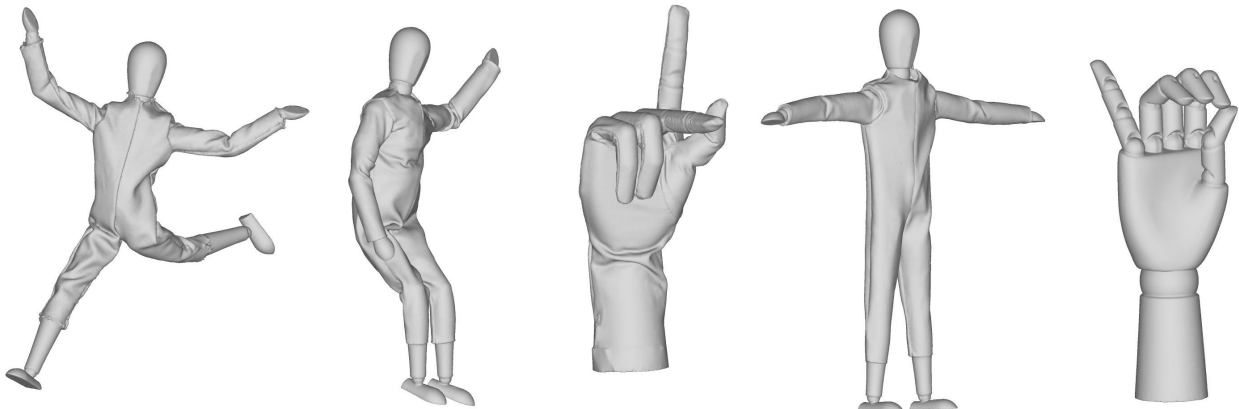[12]Department of Computer Science, Swansea University, UK
*Track organisers

Figure 1: Examples of objects in the dataset

Abstract

The registration of surfaces with non-rigid deformation, especially non-isometric deformations, is a challenging problem. When applying such techniques to real scans, the problem is compounded by topological and geometric inconsistencies between shapes. In this paper, we capture a benchmark dataset of scanned 3D shapes undergoing various controlled deformations (articulating, bending, stretching and topologically changing), along with ground truth correspondences. With the aid of this tiered benchmark of increasingly challenging real scans, we explore this problem and investigate how robust current state-of-the-art methods perform in different challenging registration and correspondence scenarios. We discover that changes in topology is a challenging problem for some methods and that machine learning-based approaches prove to be more capable of handling non-isometric deformations on shapes that are moderately similar to the training set.

CCS Concepts

• ***Theory of computation*** → *Computational geometry;* • ***Computing methodologies*** → *Mesh geometry models; Shape analysis;*

1. Introduction

Estimating the correspondence between two 3D shapes is a fundamental problem in Computer Graphics and Computational Geometry. Shape correspondence is closely related to surface registration; where shape correspondence aims to identify corresponding points or regions between two or more shapes, surface registration aims to find a transformation to bring one shape into the same global co-oridnate system of another shape. One of the applications of surface registration is to facilitate 3D model retrieval; after alignment it becomes easier to compare shapes since the correspondence between their elements is known. Shape correspondence is also necessary in common applications such as modelling [KMP07], reconstruction [LSP08] and tracking [NFS15]. Many existing methods have been proposed for computing shape correspondence [vKZHCO11, TCL*13]. Such approaches assume surface deformations to be either: piecewise rigid, (near-)isometric and/or topologically consistent. In the literature, there are only a few public benchmark shape correspondence datasets that challenge these assumptions about deformations [BRLB14, CRB*16, LRB*16, AED*18]. Previous contests [CRB*16, LRB*16] used synthetic objects that produce deformations that are not realistic. [BRLB14, AED*18] do capture real-life objects, focusing on specific object categories (i.e., human bodies and human faces), but neither benchmark suitably considers the large range of deformation that an object may undergo simultaneously. Instead of directly generating correspondences, non-rigid registration methods tend to produce a set of local transformations that deforms one surface to align with the other. Our benchmark can also be used to evaluate such methods, by working out correspondences based on the deformed shape.

We observe that there is presently no single standard benchmark for comparing the performance of shape correspondence methods under large range of deformation conditions. This has motivated us to provide a new benchmark that is divided into distinct sets, each containing different types of deformation.

Organisation Our report is organised as follows: Section 2 describes the dataset we have constructed and our approach to evaluating the results of submissions, Section 3 describes the methods we compare in this report. Section 4 evaluates the results obtained on each test-set. Finally, Section 5 concludes with a summary of the findings of this track.

2. Dataset

For this track we have produced a new dataset from 3D scans of real-world objects, captured by ourselves using a high-precision 3D scanner (Artec3D Space Spider) designed for small objects. Each object exhibits one or more types of deformation. We classify these surface deformations into four distinct groups by level of complexity:

0. Articulating – piecewise rigid deformation
1. Bending – isometric and near-isometric
2. Stretching – isotropic and anisotropic (e.g., Fig. 2a)
3. Topologically changing – heteromorphic (i.e., shapes of different topology. e.g., Fig. 2c)

The dataset consists of wooden mannequins and wooden hands

Set name	No. of pairs	Model materials
Test-set 0	14	wooden hands
Test-set 1	26	clothed hands, clothed mannequins
Test-set 2	19	very stretched clothed mannequins
Test-set 3	17	all materials

Table 1: Test-set structure.

that are articulated. To produce other types of deformation, we have created clothes for the model from two materials. We use one material that can bend but is resistant to stretching, and another that can bend and stretch. To induce greater non-isometry, we use plasticine underneath the clothing of the model. Materials and objects have been carefully selected to incrementally introduce these deformation types so that the limitations (w.r.t. deformation type) can be clearly identified. Because the dataset consists of real-world scans, it contains geometric inconsistencies and topological changes due to self-contacts. The real-scans also contain natural noise, varying triangulation of shapes and occluded geometry (e.g., Fig. 2b). Some examples of challenges are shown in Fig. 1.

A total of 76 shape pairs were selected for the test-sets (Table 1). Test-set 0 contains 14 pairs of articulating wooden hand objects. Test-set 1 contains 26 pairs of models, comprising clothed humans and hands. Test-set 2 contains 19 pairs of models; the pairings are between a thin wooden model and a larger wooden model, ensuring significant non-isometry. Test-set 3 contains 17 carefully selected pairs that contain challenging geometric and topological changes.

Information of the data underpinning the results presented here, including how to access them, can be found in the Cardiff University data catalogue (http://doi.org/10.17035/d.2019.0072003316).

2.1. Ground truth construction

To generate ground-truths, clearly drawn texture marks (Fig. 3) were made on the surfaces of the objects used. Correspondences were initially automatically determined using the shape texture maps, and then manually corrected by multiple annotators to ensure ground-truths were accurate for this track (see examples of the ground truth obtained in Fig. 4).

2.2. Evaluation

Similarly to other shape correspondence benchmarks [CRB*16, LRB*16], the correspondence quality of each method is evaluated using the evaluation procedure of [KLF11]. The quality of shape correspondence has been evaluated automatically by measuring normalised geodesics between the ground-truth and predicted correspondence. Specifically, let $(\boldsymbol{x}_i, \boldsymbol{y}_i) \in X \times Y$ be a pair of correspondences between surfaces X and Y, the normalised geodesic error ε_i between the predicted correspondence $\boldsymbol{y}_i$ and the ground truth position $\boldsymbol{g}_i$ on surface Y is measured as:

$$\varepsilon_i = \frac{d_Y(\boldsymbol{y}_i, \boldsymbol{g}_i)}{\text{area}(Y)^{1/2}} \tag{1}$$
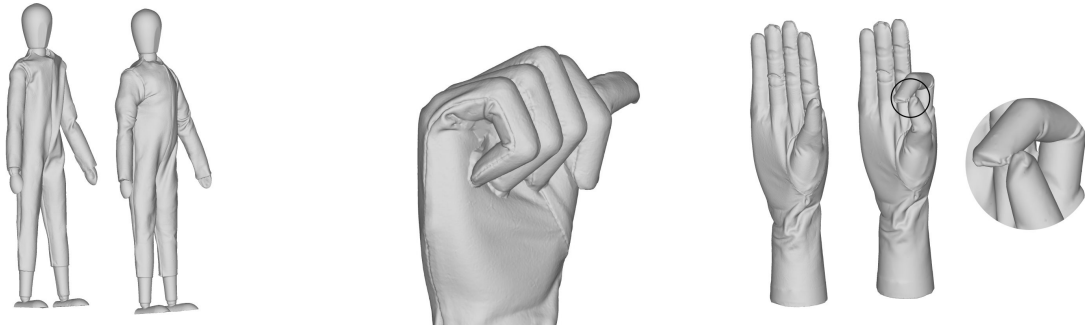
(a) Non-isometric deformation due to inflation.   (b) Geometric change caused by occlusion.   (c) Topological change caused by self-contact.

Figure 2: Illustrations of some of the challenges in our dataset.

Figure 3: A photo of the real wooden hand used in the dataset after markers were drawn.

The following measurements are used to evaluate the performance of each method:

- An overall error measurement, for methods that complete all test-sets.
- Four plots (one for each test-set) of cumulative geodesic error to demonstrate the performance of methods for individual types of deformation. This is also useful for participants that have not submitted results for all test sets.

3. Correspondence methods

This section presents the approaches used to find correspondences on one or more of the test-sets. Seven methods were evaluated using the benchmark, namely: traditional *non-rigid Iterative Closest Point* (N-ICP) [BP13], anisotropic non-rigid registration [DLRT19], deep learning-based shape correspondence [GFK*18], non-isometric partial functional maps [VLB*17], non-rigid registration with reweighted sparsity [LYLG18], genetic optimisation-based (near-)isometric shape

correspondence [Sah18], and a commercial non-rigid warping tool [Rus18].

3.1. Traditional Non-Rigid ICP (N-ICP)

To provide an effective baseline to compare the performance of the recently developed approaches we use a version of the well known N-ICP method [BP13] that has extended the original rigid formulation of ICP [BM92]. The method repeatedly applies the following two steps until convergence. In the first step, it finds correspondences between surfaces based on closest point matching, similar to ICP. In the second step, to align surfaces the method minimises distances between correspondences; point-to-point distances are combined with point-to-plane distances to speed up the convergence. It also uses 1-ring as-rigid-as-possible regularisation to smooth local deformations.

3.2. Non-Rigid Registration with Anisotropic Estimation (R. Dyke, Y.-K. Lai, P. L. Rosin & G. K. L. Tam)

The method [DLRT19] follows the N-ICP framework that alternately improves correspondences and local transformations. The initial correspondences are obtained based on matching of local geometric features (SHOT [TSDS10] is used). In order to address (local) anisotropic deformations, the method iteratively estimates local anisotropy (represented as local principal directions and principal scaling factors), which is then incorporated in an extended diffusion pruning framework [TMRL14] to identify consistent correspondences, taking anisotropy into account when calculating geodesic distances. Local regions with substantial stretching may end up with very few correspondences identified due to changes of local geometric features. To cope with significantly different input shapes, the method further introduces additional correspondences by taking existing correspondences as landmarks.

3.3. 3D-CODED (T. Groueix, M. Fisher, V. G. Kim, B. C. Russell & M. Aubry)

The method in [GFK*18] takes a deep learning approach for matching deformable shapes, and introduces Shape Deformation Networks which jointly encode 3D shapes and correspondences.

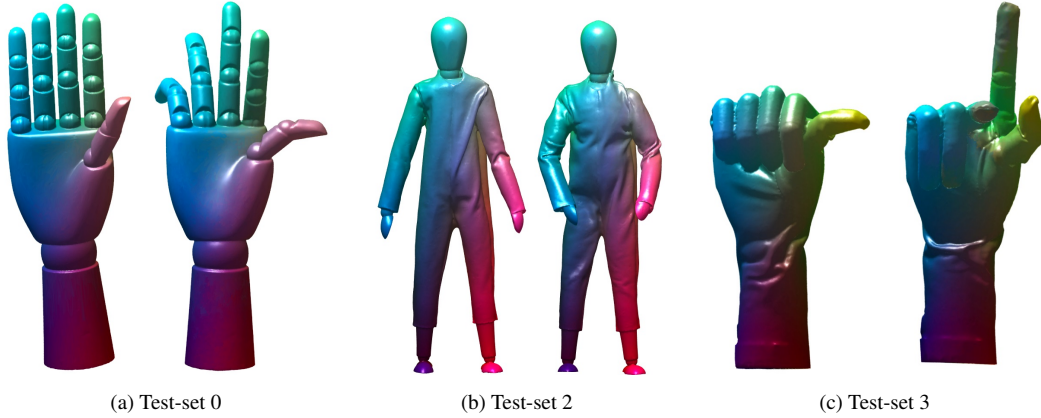(a) Test-set 0   (b) Test-set 2   (c) Test-set 3

Figure 4: Shape pair from test-sets 0, 2 & 3 with ground truth correspondences visualised.

This is achieved by factoring the surface representation into (i) a template that parameterises the surface, and (ii) a learnt global feature vector that parameterises the transformation of the template into the input surface. By predicting this feature for a new shape, correspondences between this shape and the template are implicitly predicted. These correspondences can be improved by an additional step which improves the shape feature by minimising the Chamfer distance between the input and transformed template.

To learn a transformation between shapes, an encoder-decoder architecture is trained end-to-end to optimise a regularised reconstruction loss. 3D shape correspondences between two shapes X and Y are found by first using the decoder to compute the parameters that deform the template to each of the two shapes. For each point on shape X, its nearest neighbour is found on the template deformed to X. This template point has a known corresponding point in the template deformed to Y, which is then used to find the nearest neighbour in Y.

The hyperparameters were unchanged for all the tests. The code used is available online from the authors of 3D-CODED [Gro18] and the pre-trained network called: "sup_human_invY_network_last.pth" was used. An example output of the deformed template using this method is shown in Fig. 5.

3.4. Kernel Matching (M. Vestner, Z. Länher, A. Boyarski, O. Litany, R. Slossberg, T. Remez, E. Rodolà, A. M. Bronstein, M. M. Bronstein, R. Kimmel & D. Cremers)

Kernel Matching applies the method proposed in [VLB*17] using the publicly available code [Lae17]. The algorithm solves a series of linear assignment problems (LAPs) of the form

$$\mathbf{P}^{(k+1)} = \underset{\mathbf{P} \in \Pi_n}{\arg\max} \langle \mathbf{P}, \alpha \mathbf{F}_{\mathcal{Y}} \mathbf{F}_{\mathcal{X}}^\top + \mathbf{K}_{\mathcal{Y}}^{t_k} \mathbf{P}^{(k)} \mathbf{K}_{\mathcal{X}}^{t_k} \rangle \qquad (2)$$

$$\mathbf{P}^{(0)} = \underset{\mathbf{P} \in \Pi_n}{\arg\max} \langle \mathbf{P}, \alpha \mathbf{F}_{\mathcal{Y}} \mathbf{F}_{\mathcal{X}}^\top \rangle \qquad (3)$$
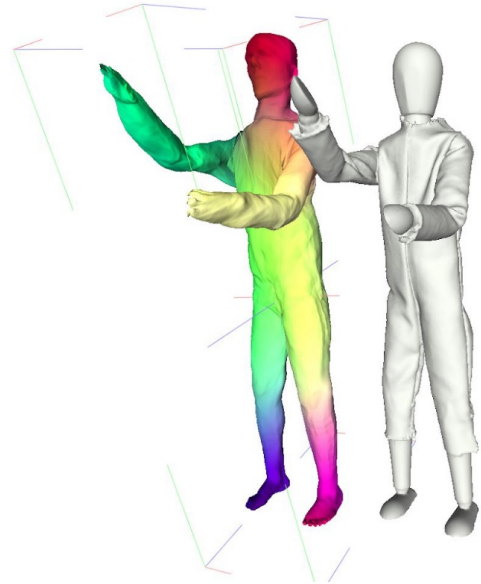

Figure 5: This figure shows an example output of the deformed template using [GFK*18].

where $\mathbf{P}$ is a permutation matrix, $\mathbf{F}_{\mathcal{X}}, \mathbf{F}_{\mathcal{Y}}$ are matrices of point-wise descriptors and $\mathbf{K}_{\mathcal{X}}^{t_k}, \mathbf{K}_{\mathcal{Y}}^{t_k}$ are the positive-definite heat kernel matrices with diffusion parameter t_k on shapes $\mathcal{X}$ and $\mathcal{Y}$, respectively. Intuitively, the first term in Eqn. 2 describes descriptor similarity and the second how well the neighbourhood information is preserved by comparing heat kernels. With decreasing diffusion parameter more emphasis is put on local neighbourhoods (cf. ε/δ in def. of continuity). The paper gives more details about connections to quadratic assignment problems of the form

$$\underset{\mathbf{P} \in \Pi_n}{\arg\max} E(\mathbf{P}) = \underset{\mathbf{P} \in \Pi_n}{\arg\max} \langle \mathbf{P}, \alpha \mathbf{F}_{\mathcal{Y}} \mathbf{F}_{\mathcal{X}}^\top + \mathbf{K}_{\mathcal{Y}}^{t_k} \mathbf{P} \mathbf{K}_{\mathcal{X}}^{t_k} \rangle \qquad (4)$$

as well as interpretations in terms of *kernel density estimation* and *low pass filtering of correspondences*.

By construction the algorithm yields bijections and is – in its basic variant – only applicable to pairs of shapes with consistent sampling, in particular with the same number of vertices. In addition solving the LAP becomes intractable for high number of vertices.

We thus apply a multi-scale approach that overcomes both issues: At each scale a subset of the vertices is sub-sampled (with increasing density). The solution of each scale induce Voronoi cells in the following scale, and sparse initial correspondences for the next scale.

Since the Voronoi cells can directly be put into correspondence, we match the vertices between corresponding cells and thus solve a set of smaller LAPs instead of one big LAP. Notice that the payoff matrices (Eqn. 2) of an LAP capture the correspondences between the centres of all Voronoi cells. The different number of vertices within corresponding cells can be tackled via slack variables. As a consequence the final matching is a bijection between subsets of the vertices on $\mathcal{X}$ and $\mathcal{Y}$. The fraction of unmatched vertices is low and tends to appear in areas with inconsistent sampling.

Two sets of results were submitted for this method with different parameters. The diffusion parameters for heat kernels remained the same throughout the benchmark. After normalising the shapes to have unit surface area, the diffusion parameters are set to

$$(\underbrace{\log_{10}(500),\ldots,\log_{10}(500)}_{3x},\ldots,\underbrace{\log_{10}(10),\ldots,\log_{10}(10)}_{3x}) \quad (5)$$

10, logarithmic sampling

Parameters for SHOT results As pointwise descriptors we use SHOT [TSDS10] as described in the paper.

Parameters for SHOT & HKS results We use SHOT [TSDS10] and HKS [SOG09] as pointwise descriptors.

3.5. Reweighted Position and Transformation Sparsities (K. Li, J. Yang, Y.-K. Lai, D. Guo, Z. Wu)

In order to cope with challenges of non-rigid registration, namely high degrees of freedom and presence of noise and outliers, [LYLG18] proposes a robust non-rigid registration method using reweighted sparsities on position and transformation to estimate the deformations between 3D shapes. Observing that large position and transformation errors tend to concentrate on local areas, which can be considered as sparse signals over surfaces, they formulate the energy function with position and transformation sparsity on both the data term and the smoothness term, and define the smoothness constraint using local rigidity. The double sparsity based non-rigid registration model is enhanced with a reweighting scheme to further improve its robustness. The formulation is solved by transferring it into four alternately-optimised sub-problems which have exact solutions and guaranteed convergence. To cope with large differences in source and target shapes, diffusion pruning [TMRL14] is applied to obtain initial correspondences based on matching of local SHOT features [TSDS10], and further correspondences are introduced during iterative optimisation based on closest points, similar to the standard N-ICP framework.
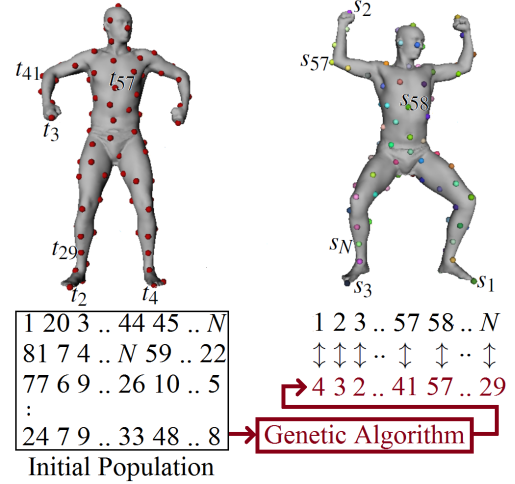

Figure 6: Overview of the genetic algorithm [Sah18].

3.6. Genetic Isometric Shape Correspondence (Y. Sahillioğlu)

The method in [Sah18] exploits the permutation creation ability of genetic optimisation to find the permutation matrix that encodes correspondences between two point sets. To this end, Sahillioğlu provides a genetic algorithm for the 3D shape correspondence problem. The point sets to be matched are sampled from two isometric (or near-isometric) shapes. The sparse one-to-one correspondences produced by this algorithm minimises the following isometric distortion function:

$$\mathcal{D}_{\text{iso}}(\phi) = \frac{1}{|\phi|} \sum_{(s_i,t_j)\in\phi} \frac{1}{|\phi'|} \sum_{(s_l,t_m)\in\phi'} |d_{\text{g}}(s_i,s_l) - d_{\text{g}}(t_j,t_m)| \quad (6)$$

where $d_{\text{g}}(.,.)$ is the normalised geodesic distance between two points on a given surface and $\phi' = \phi \setminus \{(s_i,t_j)\}$ in the most general setting. The optimal bijection ϕ^* being sought minimises $\mathcal{D}_{\text{iso}}$ in the huge space of all $N!$ possible bijections while matching N points. Since a bijection is merely an assignment of a permutation π of the target samples to the fixed source samples, the proposed genetic algorithm efficiently seeks the optimal permutation π^* of indices that will be used as subscripts of $\{t_j\}$, e.g., fixed $s_1, s_2, .., s_N$ is assigned to $t_4, t_3, .., t_{29}$, respectively, and $\pi^* = 4, 3, .., 29$ (Fig. 6).

Having represented a permutation that defines a correspondence as a chromosome, [Sah18] evolves with a fitness function that yields the set of correspondences with minimal distortion using carefully designed genetic operations. The algorithm with the same parameters used in the original paper is able to compute correspondences under articulated, isometric, and non-isometric deformations of this dataset. Two sets of results were submitted for this method with different levels of sparsity, one set that has relatively sparse correspondences ($\tilde1$00 per shape pair) and one set of extremely sparse correspondences (6 per shape pair). A random result from each deformation type is shown in Fig. 7.
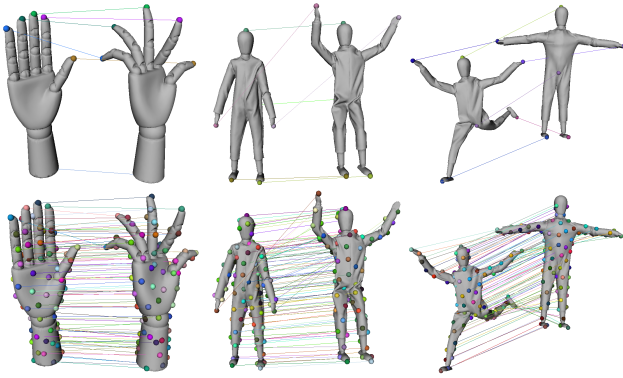
Figure 7: Extremely sparse (top) and sparse (bottom) correspondences produced by [Sah18] on some pairs.

3.7. RSDS Wrap 3.3

Wrap 3 [Rus18] is a widely used commercial software tool for mesh processing that includes a wrapping tool that non-rigidly fits one 3D shape to another. It is often used to wrap a well structured base mesh around unstructured scanned data. This method accepts pre-defined point correspondences between shapes to create control nodes on the source shape. For consistency, we also use the diffusion pruning [TMRL14] method to generate an initial set of correspondences for initialisation. A position for each control node is then found so that it matches the target shape as closely as possible. The method runs iteratively where the density of control nodes is increased per iteration. This leads to an approximation of the target shape with increasing accuracy per iteration.

4. Results & discussion

Here we present quantitative results of the method described in Section 3. Figs. 8 to 11 show the geodesic error of correspondences generated by each method on each test-set. Fig. 12 shows the combined results for methods that registered all test sets. Table 2 reports the percentage (and where appropriate number) of correspondences returned by each method. Table 3 shows the *area under the curve* (AUC) of each method on each test-set.

Sparsity of correspondence results Most methods evaluated here compute a reasonably dense set of matches. The number of correspondences returned by respective methods is reported in Table 2, 100% indicates that a correspondence was found all vertices of X. As discussed in Section 3, [Sah18] submitted two sets of results, the first set consisting of an average number of 98.3 (to one decimal place) sparse correspondences, the other containing 6 correspondences. Methods [LYLG18, DLRT19, BP13, Rus18] produce a deformed source mesh towards the target mesh. We use the following strategy to work out the correspondences: For each vertex on the deformed mesh, we work out its foot point when projecting it onto the target mesh surface. This is usually located within a triangle, and the barycentric coordinates are recorded. We also reject correspondences that have a projection distance larger than the average mesh edge length, as this indicates regions where surfaces are not

accurately aligned. We note that before rejecting correspondences, we observe that the overall results of "all test sets" for [LYLG18] & [DLRT19] were comparable.

Test-set 0 This set contains only articulated deformations. This is the most simple type of deformation that we investigate. Thus we expected most methods to perform well on this test-set. However, we discover performance varies across many methods, especially when compared to the other test-sets. Inspecting the shapes in the dataset reveals that the surfaces are primarily comprised of smooth surfaces that lack high frequency geometric details. For example finger regions (cylinder-like surfaces) are symmetrically ambiguous (see Fig. 13). This may affect the initial correspondences leading to a higher error rate. [LYLG18] performs well because the large smooth surfaces fit the sparsity assumption.

Test-set 1 This test-set contains shape pairs that bend either isometrically or near-isometrically. In it, we observed the largest difference between the best performing method ([LYLG18]) and the worst performing method (baseline N-ICP [BP13]). Shape pairs also have large-scale deformations, which typical N-ICP methods ([BP13]) cannot handle as N-ICP requires two shapes to have a good initial alignment to ensure optimal registration.

For [Sah18], the performance degrades on shape pairs of mannequins that possess bilateral symmetry. A high degree of sensitivity to the geodesic distances produced was observed on test-set 0 & test-set 1 between shape pairs where unnatural shortcuts, caused by geometric change, were present. We note that the performance of [Sah18] would have improved significantly if such problematic pairs (flips and shortcuts) were discarded.

Test-set 2 We observe the fastest convergence to 100% from [GFK*18]. It should be noted that this test-set contains only non-isometric human models. [GFK*18] demonstrates how the use of a pre-trained network from some datasets may be generalised for other datasets. With respect to the other methods, we observe that SHOT-based approaches suffer significantly, when compared with the results in test-set 0 and test-set 1. We expect that this is caused by the non-isometry. As SHOT signatures are not well defined for such non-isometric surfaces, the degradation in performance is reasonable.

Test-set 3 [VLB*17] achieves notably worse results through the combination of SHOT and HKS when compared with using SHOT, whereas for test-set 2 using SHOT and HKS performs better on the contrary. This demonstrates the instability of HKS under topological change. Topological changes appear to be challenging, and likely to be beyond the assumptions of most methods. Therefore, some methods did not participate in this test. However, for those that participated in this test-set, the overall AUC appears comparable to other test-sets. This is probably because, apart from topological changes, this test-set tends to have less distortion.

5. Conclusions

In this paper we have presented a novel dataset of real-world scanned objects that cover a large variety of deformation types. Our
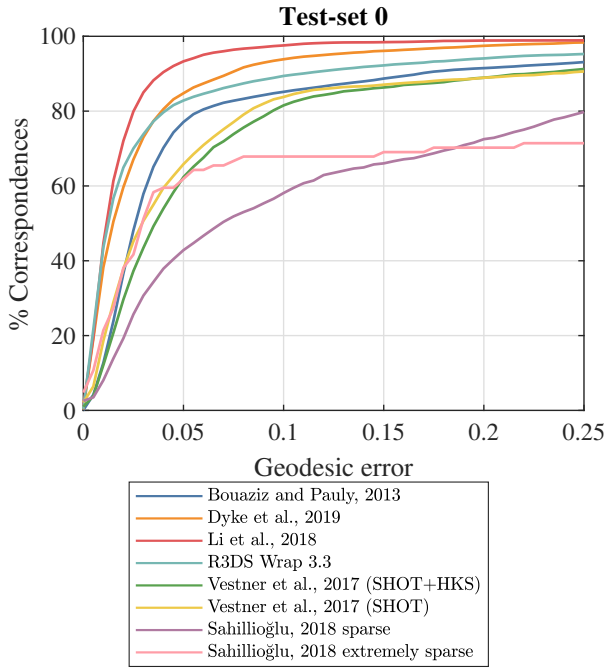
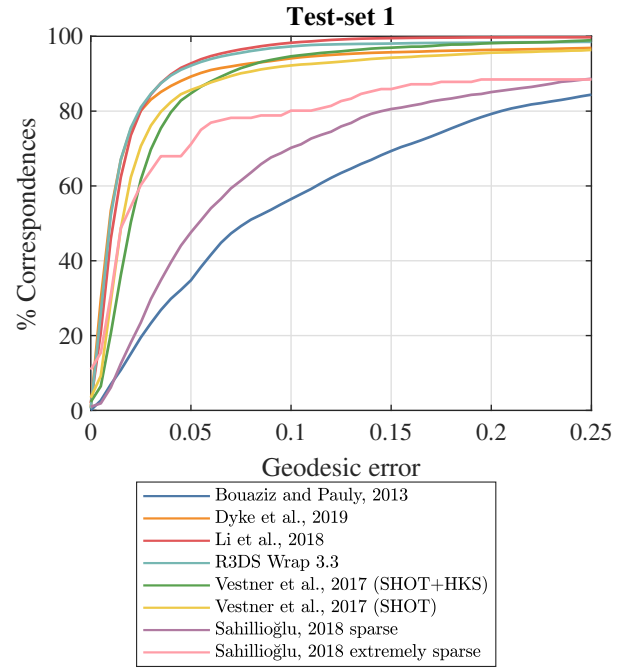Figure 8: Results for test-set 0.

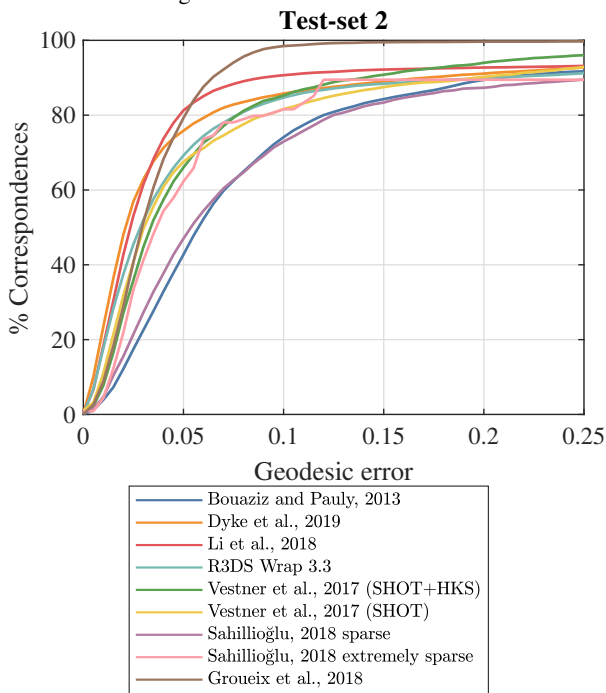Figure 9: Results for test-set 1.
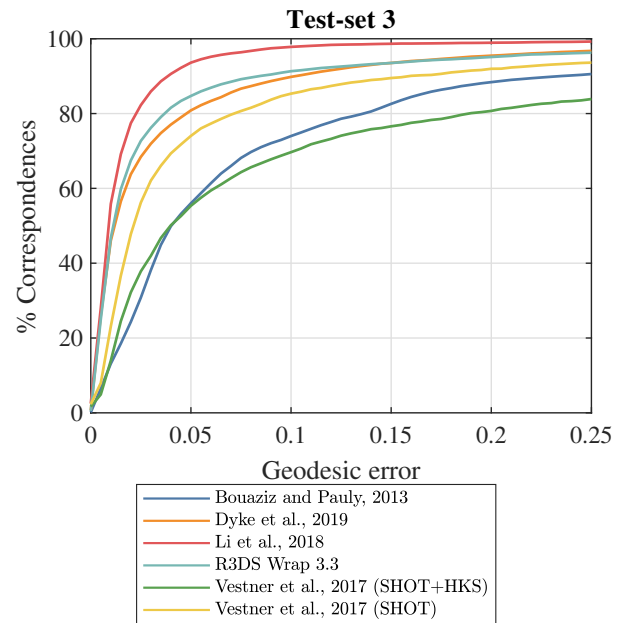

Figure 10: Results for test-set 2.

Figure 11: Results for test-set 3.

investigation has found that changes in topology is a challenging problem for some methods.

Machine learning-based approaches prove to be more capable of handling non-isometric deformation. However, they often associate with high training cost, and may not generalise to arbitrary data. Recent advances in non-rigid registration techniques that explicitly model non-isometric deformation generally perform well in many scenarios. Though they do not perform as good as deep learning techniques in non-isometric deformation, they do not require training, are generically applicable to unseen datasets, and

Method	Correspondences
[DLRT19]	99.02%
[LYLG18]	75.96%
[BP13]	49.64%
[Rus18]	93.99%
[VLB*17] (SHOT+HKS)	92.31%
[VLB*17] (SHOT)	92.39%
[GFK*18]	100%
[Sah18] sparse	98.34
[Sah18] extremely sparse	6

Table 2: Sparsity of correspondence results given as either a percentage of the number of vertices in shape *X* or the number of correspondences, where appropriate.

are less susceptible to topological changes. There is also a need to develop more reliable features for point-based correspondence on non-rigid surfaces.

To summarise, our experimental results suggest that developing correspondence techniques that are generic, reliable to any kind of seen/unseen deformation and surface, whilst handling noise and topological changes are still an on-going challenge. No single technique is perfect, but the results would also indicate an interesting direction: combining the individual advantages of sophisticated deep learning models and the advantages of generic non-rigid non-isometric registration techniques may lead to a more useful and generic correspondence technique that performs well in most scenarios, and would practically be applicable in downstream applications.

It is interesting to see how well a commercial solution compares to the state-of-the-art methods.

Through this track we have discovered some challenges in fairly evaluating the performance of shape correspondence methods. Taking intrinsic symmetries of shape into account and reporting details, such as the sparsity of correspondences estimated, need further investigation.

Further exploration of the robustness of shape correspondence methods on partial real scans would be interesting, and our dataset could be augmented to provide such challenges in the future.

Acknowledgements

References

[AED*18] ANDREWS G., ENDEAN S., DYKE R., LAI Y., FFRANCON G., TAM G. K. L.: HDFD - A high deformation facial dynamics benchmark for evaluation of non-rigid surface registration and classification. *CoRR abs/1807.03354* (2018). arXiv:1807.03354. 2

[BM92] BESL P. J., MCKAY N. D.: A method for registration of 3-D shapes. *IEEE Transactions on Pattern Analysis and Machine Intelligence 14*, 2 (1992), 239–256. doi:10.1109/34.121791. 3
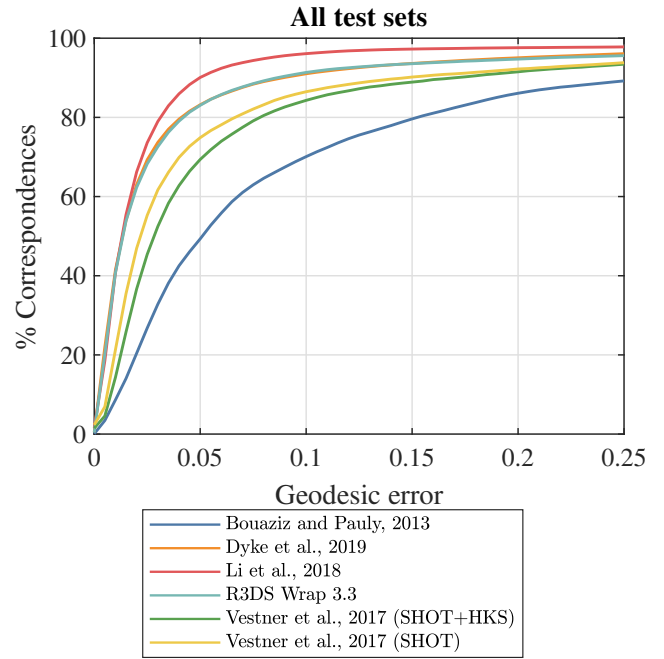

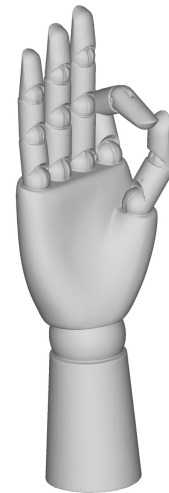Figure 12: Results for all test-sets.

Figure 13: Wooden hand object from the dataset that illustrates the lack of high frequency geometric details on the shape's surface.

[BP13] BOUAZIZ S., PAULY M.: Dynamic 2D/3D registration for the Kinect. In *ACM SIGGRAPH 2013 Courses* (New York, NY, USA, 2013), SIGGRAPH '13, ACM, pp. 21:1–21:14. doi:10.1145/2504435.2504456. 3, 6, 8, 9

[BRLB14] BOGO F., ROMERO J., LOPER M., BLACK M. J.: FAUST: Dataset and evaluation for 3D mesh registration. In *IEEE Conference on Computer Vision and Pattern Recognition* (June 2014), pp. 3794–3801. doi:10.1109/CVPR.2014.491. 2

[CRB*16] COSMO L., RODOLÀ E., BRONSTEIN M. M., TORSELLO A., CREMERS D., SAHILLIOĞLU Y.: Partial matching of deformable shapes. In *Proceedings of the Eurographics Workshop on 3D Ob-*

	test-set 0	test-set 1	test-set 2	test-set 3	all test sets
[LYLG18]	**0.9198**	**0.9259**	0.8239	**0.9286**	**0.8992**
[DLRT19]	0.8784	0.8986	0.8011	0.8583	0.8615
[Rus18]	0.8532	0.9199	0.7725	0.8698	0.8595
[VLB*17] (SHOT)	0.7601	0.8651	0.7566	0.7992	0.8039
[VLB*17] (SHOT+HKS)	0.7391	0.8710	0.7763	0.6638	0.7767
[BP13]	0.7901	0.5720	0.6750	0.7033	0.6673
[Sah18] sparse	0.5654	0.6595	0.6743	–	–
[Sah18] extremely sparse	0.6300	0.7763	0.7459	–	–
[GFK*18]	–	–	**0.8605**	–	–

Table 3: The resulting AUC for each method on each test set. Rows are in descending order of score over all test sets.

ject Retrieval (2016), 3DOR '16, Eurographics Association, pp. 61–67. doi:10.2312/3dor.20161089. 2

[DLRT19] DYKE R. M., LAI Y., ROSIN P. L., TAM G. K. L.: Non-rigid registration under anisotropic deformations. *Computer Aided Geometric Design* (2019). 3, 6, 8, 9

[GFK*18] GROUEIX T., FISHER M., KIM V. G., RUSSELL B. C., AUBRY M.: 3D-CODED: 3D correspondences by deep deformation. In *The European Conference on Computer Vision (ECCV)* (September 2018). 3, 4, 6, 8, 9

[Gro18] GROUEIX T.: 3D-CODED: 3D correspondences by deep deformation. https://github.com/ThibaultGROUEIX/3D-CODED, 2018. 4

[KLF11] KIM V. G., LIPMAN Y., FUNKHOUSER T.: Blended intrinsic maps. In *ACM SIGGRAPH 2011 Papers* (2011), SIGGRAPH '11, ACM, pp. 79:1–79:12. doi:10.1145/1964921.1964974. 2

[KMP07] KILIAN M., MITRA N. J., POTTMANN H.: Geometric modeling in shape space. *ACM Trans. Graph. 26*, 3 (July 2007). doi:10.1145/1276377.1276457. 2

[Lae17] LAENHER Z.: Efficient deformable shape correspondence via kernel matching. https://github.com/zorah/KernelMatching, 2017. 4

[LRB*16] LÄHNER Z., RODOLÀ E., BRONSTEIN M. M., CREMERS D., BURGHARD O., COSMO L., DIECKMANN A., KLEIN R., SAHILLIOĞLU Y.: Matching of deformable shapes with topological noise. In *Proceedings of the Eurographics Workshop on 3D Object Retrieval* (2016), 3DOR '16, Eurographics Association, pp. 55–60. doi:10.2312/3dor.20161088. 2

[LSP08] LI H., SUMNER R. W., PAULY M.: Global correspondence optimization for non-rigid registration of depth scans. *Computer Graphics Forum 27*, 5 (2008), 1421–1430. doi:10.1111/j.1467-8659.2008.01282.x. 2

[LYLG18] LI K., YANG J., LAI Y., GUO D.: Robust non-rigid registration with reweighted position and transformation sparsity. *IEEE Transactions on Visualization and Computer Graphics* (2018). doi:10.1109/TVCG.2018.2832136. 3, 5, 6, 8, 9

[NFS15] NEWCOMBE R. A., FOX D., SEITZ S. M.: DynamicFusion: Reconstruction and tracking of non-rigid scenes in real-time. In *The IEEE Conference on Computer Vision and Pattern Recognition (CVPR)* (June 2015). doi:10.1109/CVPR.2015.7298631. 2

[Rus18] RUSSIAN3DSCANNER: Wrap 3.3. https://www.russian3dscanner.com/, 2018. 3, 6, 8, 9

[Sah18] SAHILLIOĞLU Y.: A genetic isometric shape correspondence algorithm with adaptive sampling. *ACM Transactions on Graphics 37*, 5 (2018), 175:1–175:14. doi:10.1145/3243593. 3, 5, 6, 8, 9

[SOG09] SUN J., OVSJANIKOV M., GUIBAS L.: A concise and provably informative multi-scale signature based on heat diffusion. In *Proceedings of the Symposium on Geometry Processing* (2009), SGP '09, Eurographics Association, pp. 1383–1392. doi:10.1111/j.1467-8659.2009.01515.x. 5

[TCL*13] TAM G. K. L., CHENG Z., LAI Y.-K., LANGBEIN F. C., LIU Y., MARSHALL D., MARTIN R. R., SUN X., ROSIN P. L.: Registration of 3D point clouds and meshes: A survey from rigid to nonrigid. *IEEE Transactions on Visualization and Computer Graphics 19*, 7 (July 2013), 1199–1217. doi:10.1109/TVCG.2012.310. 2

[TMRL14] TAM G. K. L., MARTIN R. R., ROSIN P. L., LAI Y.: Diffusion pruning for rapidly and robustly selecting global correspondences using local isometry. *ACM Trans. Graph. 33*, 1 (Feb. 2014), 4:1–4:17. doi:10.1145/2517967. 3, 5, 6

[TSDS10] TOMBARI F., SALTI S., DI STEFANO L.: Unique signatures of histograms for local surface description. In *Proceedings of the European Conference on Computer Vision, Part III* (2010), ECCV, Springer-Verlag, pp. 356–369. doi:10.1007/978-3-642-15558-1_26. 3, 5

[vKZHCO11] VAN KAICK O., ZHANG H., HAMARNEH G., COHEN-OR D.: A survey on shape correspondence. *Computer Graphics Forum 30*, 6 (2011), 1681–1707. doi:10.1111/j.1467-8659.2011.01884.x. 2

[VLB*17] VESTNER M., LÄHNER Z., BOYARSKI A., LITANY O., SLOSSBERG R., REMEZ T., RODOLÀ E., BRONSTEIN A., BRONSTEIN M., KIMMEL R., CREMERS D.: Efficient deformable correspondence via kernel matching. In *International Conference on 3D Vision* (2017), 3DV, pp. 517–526. doi:10.1109/3DV.2017.00065. 3, 4, 6, 8, 9